Mechanical Systems and Signal Processing 115 (2019) 147–161

Contents lists available at ScienceDirect

Mechanical Systems and Signal Processing

journal homepage: www.elsevier.com/locate/ymssp

A generic tool wear model and its application to force modeling and wear monitoring in high speed milling

Kunpeng Zhu [a,b,*], Yu Zhang [a]

[a] Institute of Advanced Manufacturing Technology, Hefei Institutes of Physical Science, Chinese Academy of Science, Huihong Building, Changwu Middle Road 801, Changzhou 213164, Jiangsu, China
[b] Institute of Precision Manufacturing, School of Machinery and Automation, Wuhan University of Science and Technology, #947 Heping Avenue, Qingshan District, Wuhan 430081, Hubei, China

ARTICLE INFO

Article history:
Received 7 January 2018
Received in revised form 24 April 2018
Accepted 25 May 2018
Available online 6 June 2018

Keywords:
Tool wear monitoring
Adjustable coefficients
Tool life
High speed milling
Milling force

ABSTRACT

Tool wear is an important factor that influence machining precision and part quality in high speed milling, and it is essential to seek a convenient method to monitor and predict tool conditions. A generic wear model with adjustable coefficients is proposed and validated in this study. In this model, three wear zones of an entire tool life are divided by critical times considering the nature of different wear stages. Additionally, the intrinsic amplitude and growth frequencies in earlier and later milling stages are explicated and elaborated to determine the tool flank wear over whole milling process. The relationship between milling force against tool flank wear is studied and identified, which provides a technical foundation for online force modeling and wear monitoring. It is shown that with inclusion of the wear factor the milling force can be predicted accurately, with 98.5% agreement with the instantaneous force model. In addition, tool life can be predicted conveniently based on the wear model. Due to adjustability of coefficients in the model, it can be generalized to various machining types and conditions.

1. Introduction

High speed milling is one of the most important high speed CNC machining processes, which is widely used to produce complex geometry and high-precision parts [1]. In these processes, tool wear mechanisms and monitoring approaches have long been concerned and studied to improve product quality. Tool wear is caused by a combination of load factors (mechanical, thermal, and chemical etc.) acting on tool flute edges [2], which consists of abrasion, adhesion, diffusion, fatigue and chemical wear. Tool wear mechanism and optimization methods of machining parameters have been widely studied [3]. For instance, the effects of cutting parameters on tool life and wear mechanisms of CBN tool were studied by Cui et al. [4], and machining parameter selection strategies were proposed to prolong tool life. Wang et al. [5] studied various tool wear mechanisms, patterns and breakage for TiSiN and TiAlN coatings with cutting lengths. When investigating the tool life of high speed ball nose end milling of Inconel 718, Sharman et al. [6] found that the primary tool wear mechanism was adhesive wear, and the coating and cutting speed affect the tool life greatly. These studies have indicated that the tool wear status

* Corresponding author at: Institute of Advanced Manufacturing Technology, Hefei Institutes of Physical Science, Chinese Academy of Science, Huihong Building, Changwu Middle Road 801, Changzhou 213164, Jiangsu, China.
E-mail address: zhukp@iamt.ac.cn (K. Zhu).

https://doi.org/10.1016/j.ymssp.2018.05.045
0888-3270/

is closely related to machining parameter variations, and an appropriate tool wear monitoring strategy improves the tool life and the productivity as a result [7].

The ability to monitor and predict tool life is important for milling tools to improve the part quality and machining productivity [8][9]. Tool life can be investigated on the basis of tool flank wear in various milling types, parameters and conditions. While there is a tool life criterion to follow in the ISO standard *Tool life testing in milling – Part 2: End milling* (ISO 8688-2:1989), many researchers re-defined it according to practical machining conditions, for example, the critical tool flank wear was determined as 300 μm [10,11] or 200 μm [12] in different machining conditions and wear deterioration phenomena. With improvement of milling conditions, the tool life could possibly be prolonged over 50% [11]. Rodrigues et al. [13] evaluated different cemented carbide grades, cutting speeds, and feed per tooth rates with face milling on nickel-based alloys, and better milling conditions could be determined to improve tool life based on the wear mechanisms. However, these empirical studies are hard to generalize, and a large amount of experiments are needed to evaluate tool wear conditions under varied cutting parameters.

To reduce the experiments and generalize the modeling approaches, many intelligent models [14] were developed for tool wear modeling and monitoring, in which signals, such as cutting force [15], vibration [16] and image [17] etc., were measured, analyzed and signal features are extracted. The features indicate tool wear conditions according to the established model between signal features and tool wear. These models are constructed mainly based on machine learning techniques, such as neural network [18,19], Bayesian networks [9], and hidden Markov model (HMM) [20] etc. The tool remaining useful life (RUL) prediction of tools was demonstrated by Drouillet et al. [18], based on the machine spindle power values with different neural network training functions, which were found to be sensitive to the tool wear in the time domain. An extended Kalman filter (EKF) is applied in tracking the tool flank wear area in wet-turning of Inconel 718 nickel-based alloy with variable feed conditions by Niaki et al. [21], and the tool wear area evolution is modelled with a 3rd order polynomial empirical function. Orra et al. [22] built an adaptive linear control system to correlate the variations of cutting force to improve tool life. Overall, with these intelligent methods, the continuity machining processes can be ensured when these methods are adopted for tool wear prediction, but the tool wear prediction models are dependent on a large amount of training or observation data for improving accuracy.

In addition to the above intelligent methods, mechanical modeling approaches, combining both advantages of empirical and analytical models, have been applied to tool wear monitoring by many researchers. A model of the tool wear rate was developed by Usui et al. [23] based on the ideas of contact mechanics and considering adhesive wear. Parameters in Usui's model were composed of the normal stress on tool, sliding velocity of chip and interfacial temperature, which were predicted by FEM simulation [24]. A wear volume rate model for adhesive wear was established by Shaw [25] based on the Taylor's empirical equation [26], which revealed the influence of the real contact area between tool and workpiece on tool wear. In high speed ball nose end milling, wear and flaking are main tool failure types, and the dominant notch wear is located near the depth of the cut line. Kasim et al. [27] developed a model to predict the wear localization, which was applied to calculate the location associated with the maximum load exerted during the cutting under varying conditions. The error between the predictive model and the actual observations was verified less than 6%. Cutting chips were used to monitor tool wear by Zhang et al. [28] in ultra-precision raster milling. Tool fracture wear characteristics can be obtained according to the relation of virtual cutting edge and wear, which is only applicable to the machining environment where cutting chip shape is regular and predictable. Tool wear evolution and its influence on the quality of machined holes in dry helical milling were studied by Li et al. [29] comprising with experimental data, but the specific wear model is not provided over milling time. These built-in mathematical models with above-mentioned approaches were restricted to specific characteristics of the tool wear, by which the tool wear cannot be simulated throughout an entire tool lifecycle.

Based on the above analysis, mechanical models of tool wear in milling are mostly concerned with the overall dynamic characteristics of the tool and machining system. However, in practical milling processes, each tool tooth has different interaction with the workpiece because of the tool run-out effect, so the milling force and tool flank wear per tooth are not consistent with each other. Hence, the estimation of flank wear per tooth would be more accurate, and its effects to the instantaneous milling force variation per tooth would provide more indications to monitor tool conditions than traditional studies. Considering properties of different wear stages divided by wear statuses, a generic explicit tool wear model that could describe tool flank wear status and predict tool life is proposed in the paper. The model parameters can be adaptively determined from limited experimental data and it could be well generalized to other milling conditions and types.

2. Modelling of milling force, tool flank wear and life

2.1. The instantaneous milling force model

As tool cutting conditions are reflected by the instantaneous milling force in high speed milling, it is essential to establish a model to study the dynamics of instantaneous force and its relation to the tool geometry variations. Without loss of generality, this study focus on ball-nose end milling. The main geometry of the 3-flute ball-nose end milling cutter with a constant helical lead is shown in Fig. 1. The hemispherical center of the cutter is *Q*, and the Cartesian coordinate system *O-xyz* is

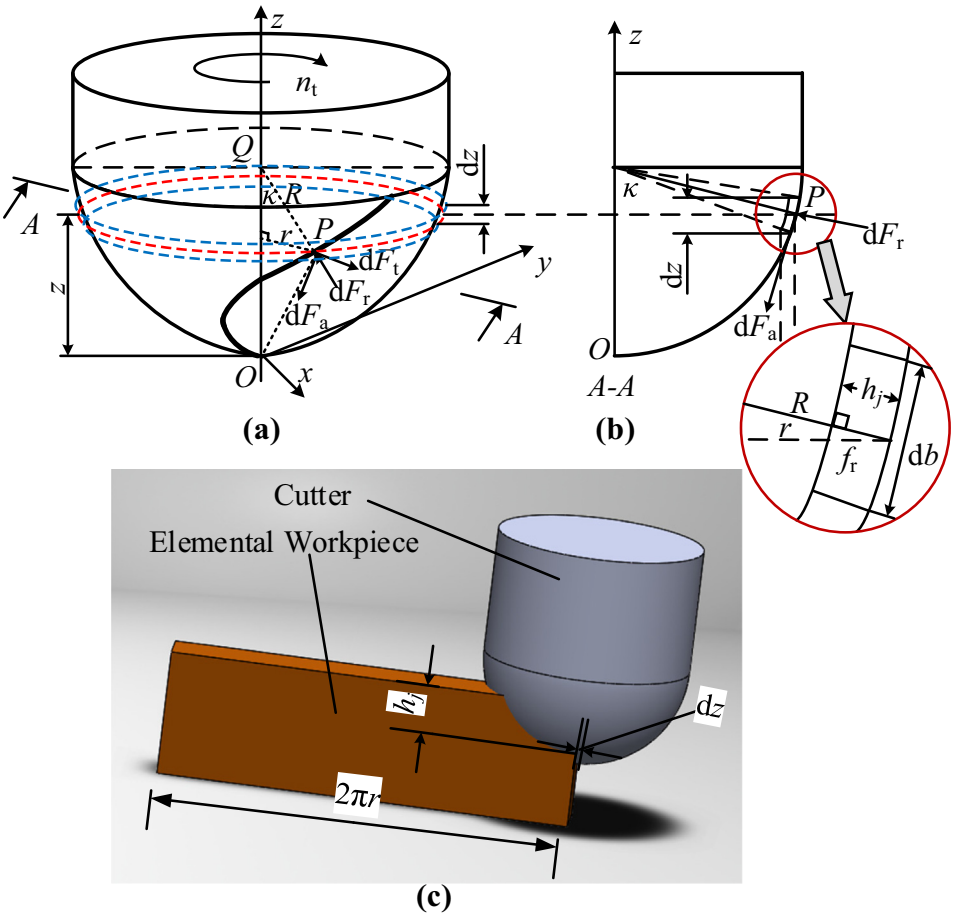

Fig. 1. Elemental model of ball-nose milling. (a) 3-Flute ball-nose milling cutter and (b) elemental chip in the front view. (c) Elemental milling model in one spindle rotation period.

established with a point O, the hemisphere vertex, as its origin. The point P is on the cutter edge of the j-th ($j = 1, 2, \ldots, N_t$) flute, where N_t is the total flutes number of the cutter, and the serial numbers of flutes are set in the counter clockwise direction. The ball-nose radius $\overline{PQ} = R$ (mm), as shown in Fig. 1a. The z-coordinate of point P is z ($z > 0$, mm). The spindle speed n_t is set in the clockwise direction.

The neighborhood at the point P in the z-axis direction is chosen as a milling element, whose length is dz (mm) on the workpiece correspondingly. The dynamic Cartesian coordinate system P-tra is established with the point P as its origin, and the t-, r- and a-axes are paralleled to the directions of instantaneous tangential, radial, and axial milling forces respectively, as shown in Fig. 1b. The elemental milling on the circumference can be regarded as cutting process on the workpiece surface, whose length l can be given as $2\pi r$ in one milling period, where r is the r-axial radius of elemental edge, as shown in Fig. 1c. According to the basic physical formulas of the instant rigidity forces [30], the elemental forces $d\boldsymbol{F}_{\mathbf{E}j}(t, z) = (dF_{tj}, dF_{rj}, dF_{aj})^T$ (All parameters of forces are in Newton (N) unless otherwise stated.) in the P-tra coordinate system of the point P are given as:

$$d\boldsymbol{F}_{\mathbf{E}j}(t,z) = \boldsymbol{K} h_j db \quad (j = 1, 2, \ldots, N_t) \tag{1}$$

where the elements in the matrix $\boldsymbol{K} = (K_{tc}, K_{rc}, K_{ac})^T$ (N/mm^2) are the milling force coefficients in the t-, r- and a-axial directions, which are determined by the identification method based on experimental data. The subscript j in symbols represents the flute number ($j = 1, 2, \ldots, N_t$), the same below. The un-deformed chip thickness h_j (mm) and the elemental chip width db (mm) are related to the geometrical parameters of the cutter.

Referring to the geometry of the cutter in Fig. 1b, the elemental chip width db in Eq. (1) is given as:

$$db(z) = dz \cdot \csc\kappa \tag{2}$$

where κ (rad, all parameters of angles in paper are in rad unless otherwise stated.), the $\angle OQP$ in Fig. 1b, is the a-axial angle of the cutter-workpiece engagement of the point P, and the csc in Eq. (2) stands for the cosecant function, csc $(x) = 1/\sin(x)$. It can be expressed as $\arccos(1 - z/R)$ when the machining type is not slotting, i.e., $z < R$; otherwise, $\kappa = \pi/2$.

The un-deformed chip thickness h_j (μm) at milling time t and coordinate z is given as [31]:

$$h_j(t,z) = \max(0, f_z \sin\phi_j \sin\kappa + \Delta h_j - \Delta h_i) \tag{3}$$

where f_z (μm/tooth) is the feed of the workpiece per tooth, and ϕ_j is the r-axial angle of the cutter-workpiece engagement. The extra un-deformed chip thicknesses Δh_j and Δh_i in Eq. (3) are caused by the tool run-out of the current j-th and previous i-th flutes respectively, which are expressed as:

$$\Delta h_k(t,z) = r_0 \sin\kappa \cos[\alpha_0 + \psi + (k-1)\phi_p] \quad (k = i,j) \tag{4}$$

where r_0 (μm) and α_0 are tool run-out length and angle, respectively, ϕ_p is the pitch angle with $\phi_p = 2\pi/N_t$, and ψ is the lag angle caused by the helical shape of flutes.

Hence, instantaneous milling force of each flute $\boldsymbol{F}_{\mathbf{M}j}(t)$ in the x-, y- and z-axes directions can be obtained by integrating the elemental forces of each layer along the z-axis as:

$$\boldsymbol{F}_{\mathbf{M}j}(t) = \int_{z_{jd}}^{z_{ju}} \boldsymbol{T} \mathrm{d}\boldsymbol{F}_{\mathbf{E}j}(t,z) \tag{5}$$

where z_{ju} and z_{jd} (mm) are the z-axial upper and lower boundaries of the instantaneous cutter-workpiece engagement, which are determined by the r-axial angle ϕ_j. The matrix $\boldsymbol{T}$ transforms the dynamic coordinate system P-tra into the fixed coordinate system O-xyz, given as $\boldsymbol{T} = \begin{pmatrix} -\cos\phi_j & -\sin\kappa\sin\phi_j & -\cos\kappa\sin\phi_j \\ \sin\phi_j & -\sin\kappa\cos\phi_j & -\cos\kappa\cos\phi_j \\ 0 & \cos\kappa & -\sin\kappa \end{pmatrix}$.

The mechanical milling force model is validated and compared with the experimental data and the generic wear model in Section 3.

2.2. Experimental setup

A series of tests were conducted on the high speed machining center MIKRON HSM600U. In these experiments, Inconel alloy 718 is chosen as the workpiece material, and the material of 3-flute ball-nose end milling tools is tungsten carbide. Conditions and parameters in milling, depth a_p (mm) of milling and spindle speed n_t (r/min), etc., are listed in Table 1.

Table 1
Conditions and parameters in milling experiments.

Test No.	a_p (mm)	a_w (mm)	f_z (μm/tooth)	n_t (rpm)	Types of milling
1	0.2	1.960	30	8000	Slotting
2	0.2	1.960	10	10,000	Slotting
3	0.2	1.960	30	10,000	Slotting
4	0.15	1.706	50	10,000	Slotting
5	0.2	1.960	50	10,000	Slotting
6	0.25	2.179	50	10,000	Slotting
7	0.2	1.960	30	20,000	Slotting
8	0.2	1.960	30	30,000	Slotting
9	0.15	0.075	50	10,000	Half immersion
10	0.2	0.100	50	10,000	Half immersion
11	0.25	0.125	50	10,000	Half immersion
12	0.15	1.874	10	10,000	Slotting
13	0.25	2.400	30	8000	Slotting
14	0.25	2.400	10	10,000	Slotting
15	0.25	2.400	30	10,000	Slotting
16	0.2	2.154	50	10,000	Slotting
17	0.25	2.400	50	10,000	Slotting
18	0.3	2.615	50	10,000	Slotting
19	0.25	2.400	30	20,000	Slotting
20	0.25	2.400	30	30,000	Slotting
21	0.2	0.100	50	10,000	Half immersion
22	0.25	0.125	50	10,000	Half immersion
23	0.3	0.150	50	10,000	Half immersion

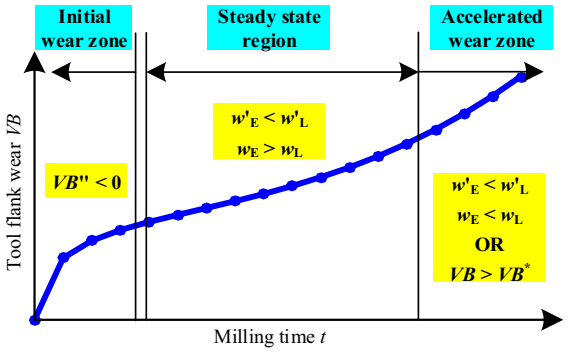

Fig. 2. Tool flank wear curve in different stages.

The instantaneous milling forces are measured by a Kistler 9265B dynamometer in 3 channels, with the sampling frequency 50KHz. Tool flank wear per tooth is measured by a LECIA MZ12.5 stereo-microscope, after finished each machining pass. The diameters of ball-nose end milling cutters are 5 mm (test No. 1–11) and 6 mm (test No. 12–23). The size of workpiece in each test is 112.5 mm × 40 mm. In order to enhance the reliability of experimental results, test 22 are repeated three times based on the same setup in Table 1, and are used as examples to validate the mechanical milling force model and the proposed tool flank wear model.

2.3. Modelling of tool flank wear with adjustable coefficients

The main forms of tool flank wear are running-in wear, adhesive wear and three-body abrasive wear sequentially [2], which are corresponding to different wear rates, respectively. In accordance with wear forms of a fresh tool in machining processes, there are three main time zones divided by critical times, that is, initial zone (I), steady state region (II) and accelerated wear zone (III). A typical tool life curve is shown in Fig. 2. The critical times are the key to estimate the working condition and lifetime of a milling tool. Determination of critical times is depended on the variations of wear rates. The first critical time is regarded as the milling time when the acceleration rate $VB'' = 0$, which is the saddle point in the tool wear curve. Two preference transition wear functions w_E and w_L are constructed for describing the wear zones II and III. In order to define the critical times, the values of transition functions' differentiations (w'_E and w'_L) are chosen as the evaluation indicator, where the functions $w'_E(t)$ and $w'_L(t)$ represent principal polynomial fitting curves of the wear rate in the initial wear zone and later wear stage respectively. Hence, the wear rate and acceleration rate, i.e., the first and second order differences VB' and VB'' of tool flank wear VB, are mainly segmented into two periods. It can be regarded as initial and significant wear stages respectively, as shown in Fig. 2.

After rapid increases of tool flank wear VB (μm), there are slight and gradual increases which followed by sharp increases. To analyze the variation tendency of tool flank wear, the wear rate and acceleration rate VB' (μm/min) and VB'' (μm/min^2) [20], as shown in Fig. 2 (experimental data), are calculated as:

$$\begin{cases} VB'(t) = \Delta VB/\Delta t = [VB(t+\Delta t) - VB(t)]/\Delta t \\ VB''(t) = \Delta VB'/\Delta t = [VB'(t+\Delta t) - VB'(t)]/\Delta t \end{cases} \tag{6}$$

where Δt (min) is an interval time of wear samplings in milling experiments, the values of tool flank wear VB are obtained from the set #1 experiment in Section 2.2.

The functions $w'_E(t)$ and $w''_L(t)$ represent polynomial fitting curves of the wear rate and acceleration rate, which are fitting the relatively regular parts in earlier and later zones in the significant wear stages correspondingly, as shown in Fig. 3 (fitting curves). In order to obtain a generic wear model, two main requirements need to be satisfied: i) The wear model is a continuously differentiable function obviously, especially at the critical times; ii) There are good agreements of the wear model both in the initial and significant wear stages with the wear curve. Based on these conditions, the expressions are then derived as:

$$w(t) = w_E(t) + w_L \tag{7a}$$

with

$$\begin{cases} w'_E = a_1/(t+b_1) + c_1 \\ w''_L = a_2 t + b_2 \end{cases} \tag{7b}$$

where a_1 (μm), a_2 (μm/min^3), b_1 (min), b_2 (μm/min^2) and c_1 (μm/min) are basic fitting coefficients. It can be found that the fitting curves have a high goodness with experimental data.

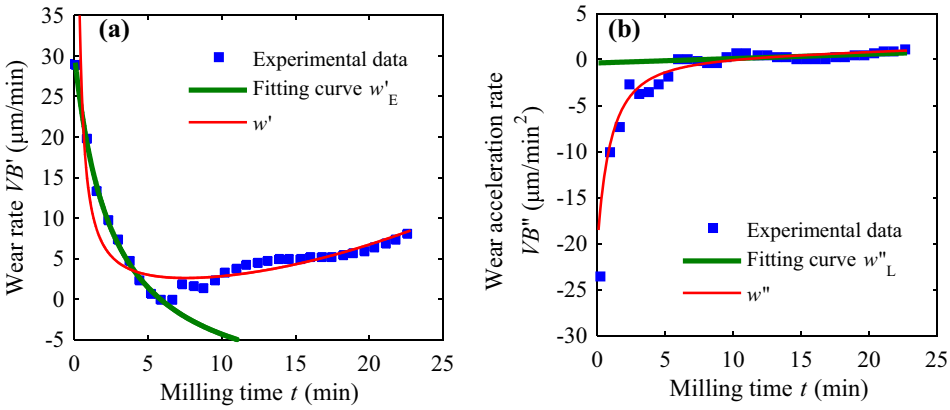

Fig. 3. Modelling with data of tool flank wear (a) rate and (b) acceleration rate over milling time. The experimental data in figures are obtained from the set #1 experiment in Section 2.2. The fitting curves w'_E and w''_L are fitted with the original experimental data, and the wear rate and acceleration rate functions w' and w'' are calculation with Eq. (7b).

In order to describe wear conditions in different stages, two functions w'_E and w''_L in earlier and later wear zones are integrated. The tool flank wear model over the milling time can be given as (See Appendix A for the derivation):

$$w(t) = w_E(t) + w_L(t) = A\ln(Bt+1) + Ct^3 \tag{8}$$

where A (μm), B (min^{-1}) and C (μm/min^3) are fitting coefficients, which are all positive. There is $w(0) = 0$ apparently. As shown in Table 2, fitting coefficients of milling experiments and the coefficient of determination R^2 show that the fitted average flank wear w has a good agreement with experimental data VB. Hence, Eq. (8) is considered as the tool flank wear model with fitting coefficients.

Based on specifications of wear curves and wear zones in Fig. 2, the milling time t is denoted as t_A when the changed rate of wear curve reached the first minimum value. The time t is denoted as t_B when effects of non- and multi order functions in the w' expression in Eq. (8) on the changed rate of wear curve are equal. When tool flank wear is less than the critical wear VB^*, the time t is denoted as t_C when effects of logarithmic and multi order functions w_E and w_L in Eq. (8) on the increase rates of tool flank wear are equal; otherwise, when $w(t) = VB^*$ the critical time t_C can be determined according to (9). Overall, the critical times, which are calculated and listed in Table 2 based on the wear data of three experiments in Section 2.2, are given as:

$$\begin{cases} w''(t_A) = 0 \\ w'_E(t_B) - w'_L(t_B) = 0 \\ t_C = \min\{\arg\min|w(t) - VB^*|,\ \arg\min|w_E(t) - w_L(t)|\} \end{cases} \tag{9}$$

There is only one set of positive real roots of Eq. (9) when $t \geq 0$. By substituting Eq. (8) and (9), the fitting coefficient B can be analytically solved considering $B > 0$, and the fitting coefficients are finally deduced as:

$$\begin{cases} B = \frac{4t_A^2 - t_B^2 + t_B\sqrt{t_B^2 + 8t_A(t_B - t_A)}}{2t_B^3 - 4t_A^3} \\ \frac{C}{A} = \frac{\ln(Bt_C+1)}{t_C^3} \end{cases} \tag{10}$$

where the critical time $t_B > \sqrt[3]{2}t_A$ because of $B > 0$.

The growth frequencies (rates) of average wear in the earlier (I) and later (III) stages are denoted as v_E and v_L (min^{-1}), with $v_E = B$ and $v_L = 1/t_C$ specifically. The fitting coefficient A can be regard as an intrinsic amplitude of average wear, and it is determined by materials of tool and workpiece and machining conditions. Hence, the generic tool average flank wear model with adjustable coefficients can be improved according to Eq. (8), which is given as:

$$w(t) = A\ln[(v_E/v_L + 1)^{(v_L t)^3} \cdot (v_E t + 1)] \tag{11}$$

Table 2
Fitting coefficients of the generic wear model with experimental data in Section 2.2.

Set No.	A (μm)	B (min^{-1})	C (μm/min^3)	t_A (min)	t_B (min)	t_C (min)	$\bar{t}$ (min)	R^2 of w
1	13.06	149.5	0.005059	7.545	9.509	27.81	33.42	0.9911
2	9.236	418.5	0.009028	5.544	6.986	21.02	28.69	0.9546
3	14.89	134.7	0.008526	6.622	8.347	24.17	27.52	0.9896

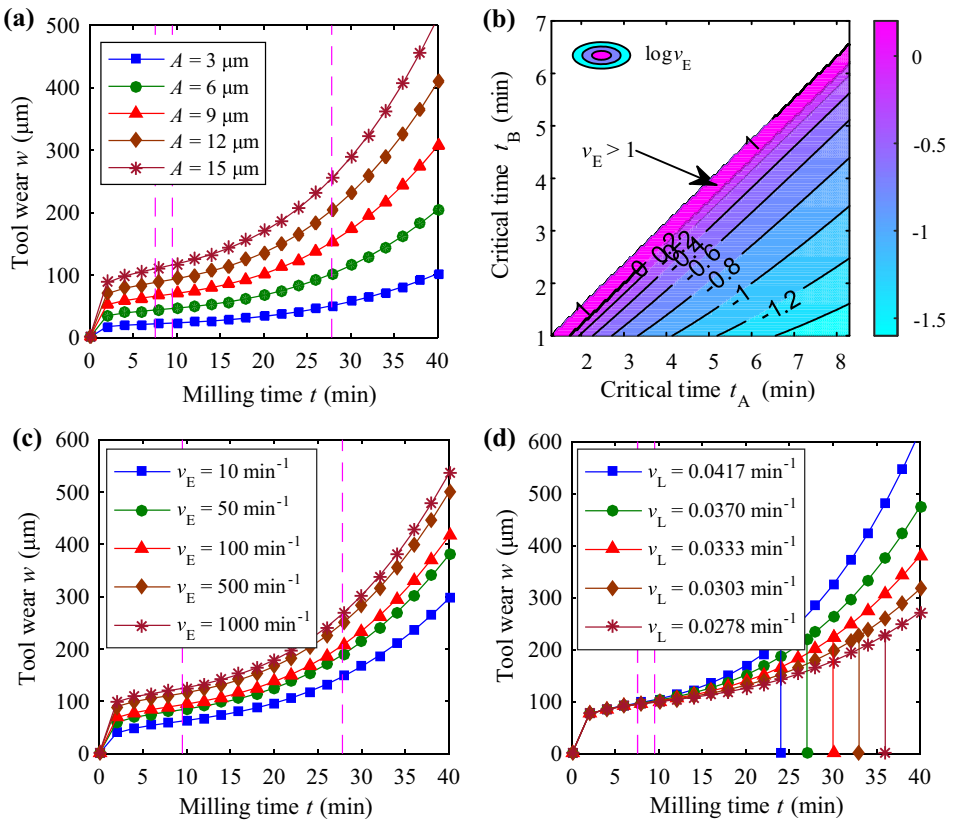

Fig. 4. Parameter analysis of tool average flank wear model with adjustable coefficients based on the first set of test 22. (a) The growth frequencies v_E = 175 min^{-1}, and v_L = 0.036 min^{-1}. (b) v_E with critical times t_A and t_B. (c) A = 13.06 μm; v_L = 0.036 min^{-1}. (d) A = 13.06 μm; v_E = 175 min^{-1}.

There are three parameters that affect tool wear in Eq. (11), A, v_E and v_L. An example study of the tool flank wear modeling with (11) is shown in Fig. 4 based on first set of test 22. The influence of the intrinsic amplitude A to average wear w is more significant with increase of milling time t, that is, good cutting conditions should enable A smaller, as shown in Fig. 4a. The growth frequency v_E in earlier wear stage is determined by the relative relationship between critical time t_A and t_B, referring to Eq. (10). Notable increasing of v_E geometrically when t_B is close to $\sqrt[3]{2}t_A$ positively is shown the contour map in Fig. 4b. The influence of v_E is reflected in the earlier wear stage of milling mainly, i.e., initial zone (I), which determines the wear condition in steady state zone (II), as shown in Fig. 4c. Thus, reducing of v_E is a good choice to increase tool average life. According to the definition, the influence of growth frequency v_L is reflected in later wear stage and is very small in earlier wear stage of milling, which is related to critical time t_C, as shown in Fig. 4d. Hence, reducing of v_L, that is, deferring milling time t_C to enter the accelerated wear zone (III), is another method to increase tool average life.

The three coefficients A, v_E and v_L in the generic tool average flank wear model are regarded as adjustable coefficients of the entire, earlier and later milling process successively, which highlight different characteristics in each stage of physical machining. Hence, the proposed tool wear model with adjustable coefficients has good adaptability in modeling tool wear under varied machining and wear conditions.

2.4. Tool life determination and force modeling with the wear model

2.4.1. Tool life determination

The critical average flank wear VB^* (μm) is set as the criterion to define an effective tool average life $\bar{t}$ (min), while VB^* is 300 μm according to the ISO standard *Tool life testing in milling – Part 2: End milling* (ISO 8688-2:1989). The tool average life $\bar{t}$ indicates the maximum time that milling tool can be used under an ideal condition (the flank wear are equal on each tool tooth), and it can be calculated by solving Eq. (11) with a critical condition, $w(\bar{t}) = VB^*$. Hence, tool average life $\bar{t}$ is obtained by numerical method according to a time set of model solutions under the critical condition:

$$\left\{\bar{t}\left|(v_E/v_L+1)^{(v_L\bar{t})^3}=\frac{\exp(VB^*/A)}{v_E\bar{t}+1}\right.\right\} \tag{12}$$

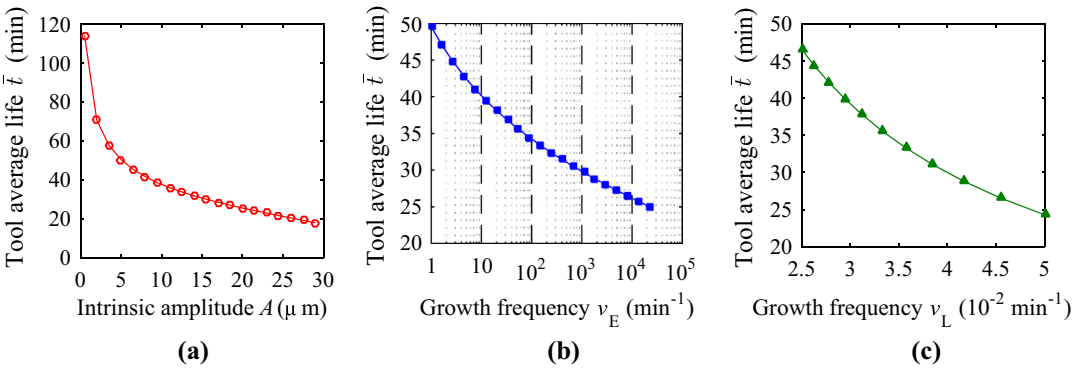

Fig. 5. Tool average life $\bar{t}$ with various adjustable coefficients based on the first set of test 22. (a) v_E = 175 min^{-1}; v_L = 0.036 min^{-1}. (b) A = 13.06 μm; v_L = 0.036 min^{-1}. (c) A = 13.06 μm; v_E = 175 min^{-1}.

The tool average life $\bar{t}$ in each set experiment is listed in Table 2. Tool life $\bar{t}$ with various intrinsic amplitudes A, growth frequencies v_E and v_L in earlier and later zones is shown in Fig. 5 respectively. Additionally, in order to facilitate the analysis, numbers on horizontal coordinate of v_E are transformed into logarithm. The increasement of $\bar{t}$ is more rapidly when the intrinsic amplitude A, growth frequencies v_E and v_L are in lower values. It can be seen that the tool average life $\bar{t}$ is improved more effectively by reducing the intrinsic amplitude A than the growth frequencies v_E and v_L (Fig. 5a). The growth frequency v_E has a larger adjusting range than A and v_L to ensure that tool average life $\bar{t}$ is long enough to meet the machining requirement (Fig. 5b). It validates the methods to increase tool average life in previous analysis.

2.4.2. The force modeling with inclusion of tool wear

Under the same machining conditions of multiple milling passes in one experiment, the growth frequencies v_E and v_L are regarded as constitutive parameters, which are related to tool and workpiece materials, milling types and parameters merely, such as feed rate v_c, milling depth a_p and ball-nose radius R, etc. The intrinsic amplitude A_j of j-th tooth is a variable over milling time t, due to the phenomenon of cutter-workpiece uneven engagement, which is related to tool run-out and machining system vibration in a milling process. Hence, according to the generic tool average flank wear model with adjustable coefficients in Eq. (11), the intrinsic amplitude per tooth $A_j(t)$ is given as:

$$A_j(t) = \frac{VB_j(t)}{\ln\left[(v_E/v_L + 1)^{(v_L t)^3} \cdot (v_E t + 1)\right]} \tag{13}$$

where $VB_j(t)$ is tool flank wear of tooth j.

The fluctuation of the intrinsic amplitude A_j in each milling pass is caused by tool calibration difference between two adjacent passes, which leads to different tool run-out and machining system vibration characteristics. Considering that the value of milling force F_j per tooth in each pass is related to cutter-workpiece engagement mainly, the percentage of F_j to the total milling force F over time t is λ_j, which can be regarded as the factor of proportionality of tool flank wear VB_j per tooth to average wear w. The wear factor λ_j is calculated by the ratio of the intrinsic amplitude A_j to the adjustable coefficient A of tool average flank wear model in Eq. (11), given as:

$$\lambda_j(t) = A_j/(AN_t) \tag{14}$$

where the factor λ_j is satisfied with the requirement of normalization, $\sum_{j=1}^{Nt} \lambda_j = 1$.

Hence, in accordance with the factor λ_j, the instantaneous milling force per tooth $F_{\mathbf{M}j}(t)$ in Eq. (5) from the mechanical force model can be estimated by combination of the generic tool flank wear model with adjustable coefficients in Eq. (11), which are given as:

$$F_{\mathbf{M}j}(t) = |\boldsymbol{F}_{\mathbf{M}j}(t)| \tag{15a}$$

$$F_j(t) = \lambda_j(t) F_{\mathbf{O}}(t) \tag{15b}$$

where $F_{\mathbf{O}}(t)$ is the experimental measurement data of milling force on a milling cutter, which is calculated according to the measured force data in x-, y- and z-axial directions by a dynamometer, as shown in Section 2.2. The correlation of milling force per tooth F_j, which is obtained from the generic tool flank wear model, with the mechanical milling force per tooth $F_{\mathbf{M}j}$ is discussed in Section 3.3.

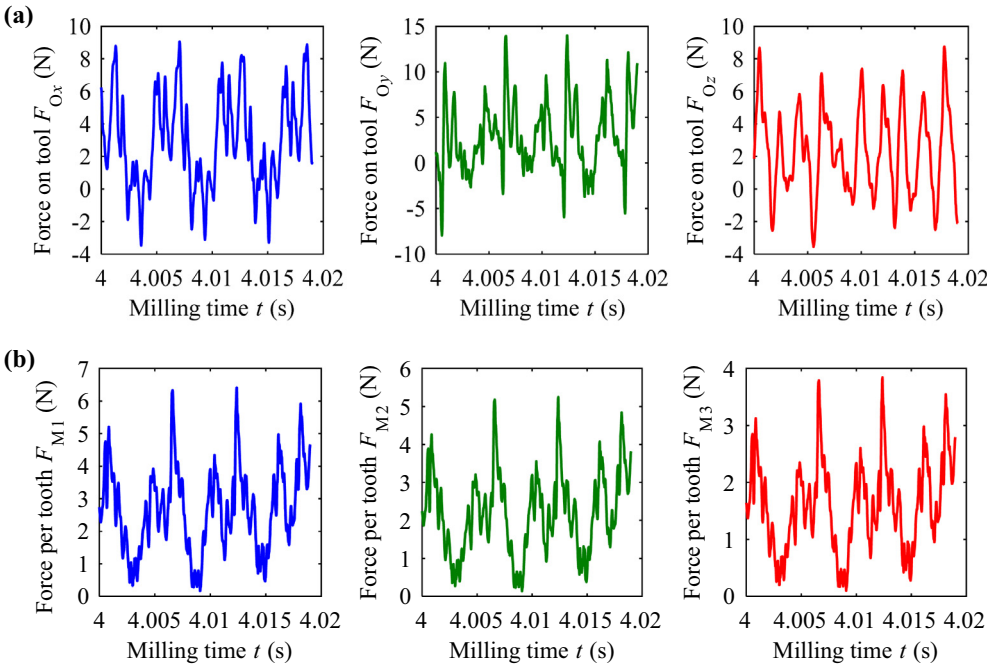

Fig. 6. Exemplary results from milling experiments. (a) Milling force of experimental data on overall tool in x-, y- and z-axial directions. (b) Milling force per tooth based on the mechanical milling force model in Eq. (15a).

3. Results and discussion

3.1. The milling force and tool flank wear

Exemplary results of experiments are illustrated in Fig. 6 with milling conditions of test 22, as shown in Table 1. The milling period $T_p = 60/n_t = 6$ ms. According to the feed f_z per tooth, the Fig. 6a shows milling forces in x-, y- and z-axial directions with over three periods, while the milling time t means start time in 10th milling pass of test 22. It indicates that the

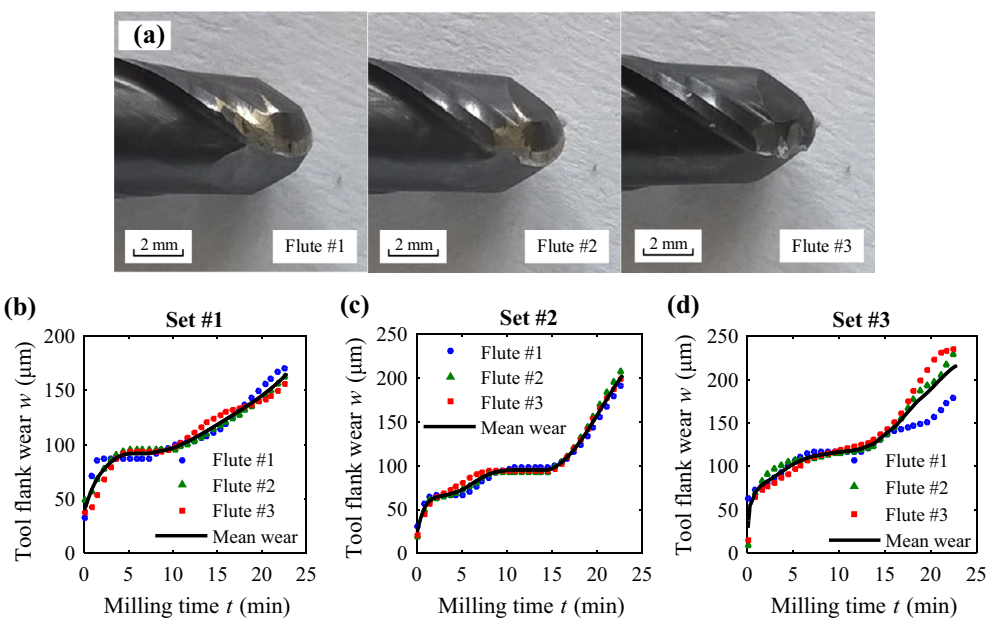

Fig. 7. (a) Tool flank wear on each flute of the set #1 experiment; wear on each flute and mean wear over milling time in the set (b) #1, (c) #2 and (d) #3.

existence of periodic vibrations and irregular interferences produce disturbance signals on milling forces, especially on the *z*-axial direction, which is sensitive to the machining system and could be further studied to characterize process stability. At the same time, considering the mechanical milling force model in Eq. (15a), which is not consistent with each other, milling force per tooth is an important feature to indicate the tool wear rate, as shown in Fig. 6b. According to Eq. (5) and cutting mechanics, the cutting force is related to the contact area between tool and workpiece, and the contact area of worn tool is determined on tool flank wear mostly in milling.

Tool flank wear VB_j per tooth over milling time in the set #1 experiment is shown in Fig. 7a. Considering the tool run-out effect and milling system dynamics in machining processes, tool flank wear per tooth is different from each other, as shown in Fig. 7b–d. The flank wear of each flutes are quite consistent in set #1 and #2, while the curve variations in Fig. 7d indicate that the flank wear on the first flute of set #3 is relatively smaller than others. At the same time, the acceleration zone of the set #3 is more fluctuated than set #1 and #2, and more wear value in the set #3 is achieved than the set #1 and #2 in the same milling time, which decreases the tool life.

The un-deformed chip thickness h_j of each flute according to Eq. (3) is simulated with slot milling in Fig. 8, which is different from others because of the tool run-out effect. The Fig. 8a shows h_j of each flute with the milling time t and *z*-coordinate z in one cycle. The maximum h_j of each flute with t in current milling conditions is shown in Fig. 8b, which reveals that the additional increase of the first and third flutes and decrease of the second flute of h_j are caused by tool run-out, and the first flute is milling the most part of the workpiece because that the run-out angle $\alpha_0 = 6°$ and it closest to the first flute. The un-deformed chip thickness h_j increases with the increase of z in same milling time t, and the time when adjacent flutes are jointly milling the workpiece increases with z too, as shown in Fig. 8c.

3.2. Tool life prediction

In practical milling process, the different tool flank wear VB_j per tooth with each other are mainly due to the tool run-out [31]. The tool average life $\bar{t}$ is related to the tool life $\bar{t}_j$ per tooth, which can be described and predicted by Eq. (12) in accordance with the intrinsic amplitude A_j in Eq. (13). The predicted tool life of three sets of test 22 over milling time t is shown in Fig. 9. The milling time t starts with a fresh tool in each set, and ends with the accomplishment of the corresponding exper-

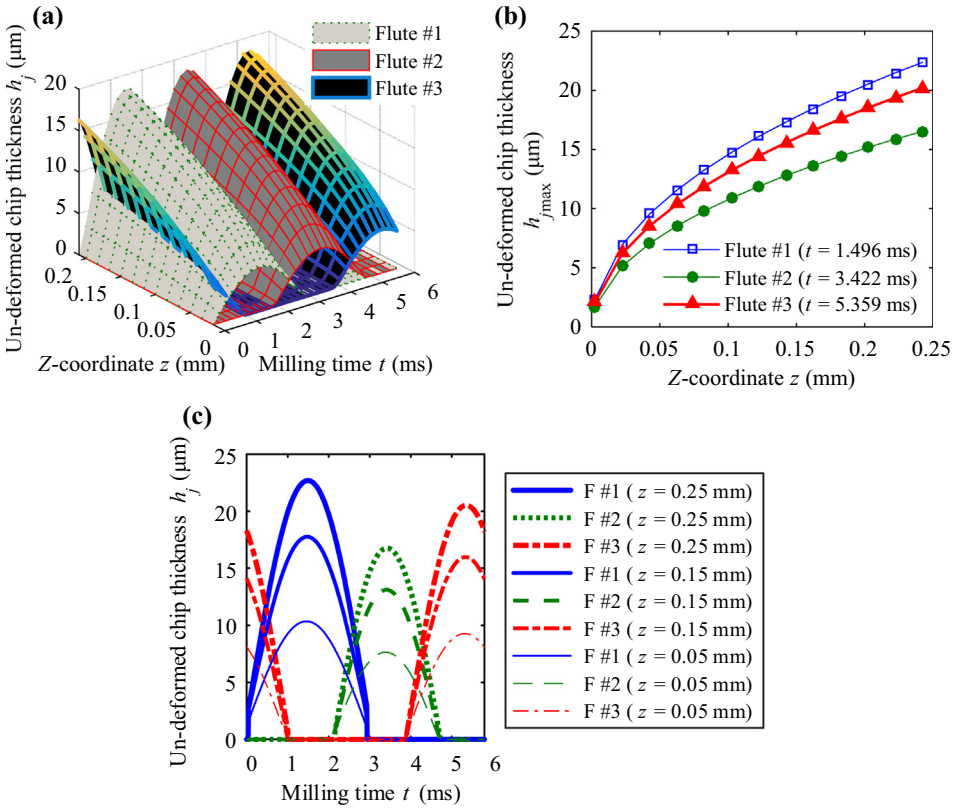

Fig. 8. Un-deformed chip thickness h_j simulation results with tool run-out length $r_0 = 5$ μm and angle $\alpha_0 = 6°$. (a) 3-dimensional graph of h_j over milling time t and *z*-coordinate z. (b) Maximum h_j of each flute with *z*-coordinate z. (c) h_j of each flute at different *z*-coordinate over milling time t.

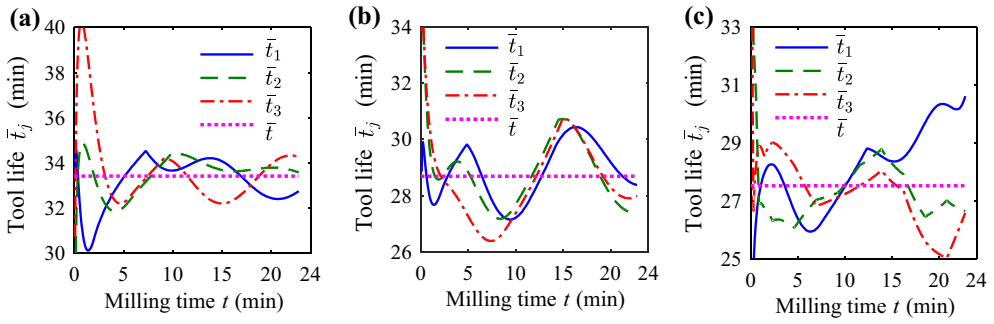

Fig. 9. Prediction of tool life over milling time t in the set (a) #1, (b) #2 and (c) #3. The tool average life $\bar{t}$ of each set is calculated by Eq. (12), and the tool life $\bar{t}_j$ on each tooth is determined according to the intrinsic amplitude A_j in Eq. (13).

iments in Section 2.2. The variation of each tool life $\bar{t}_j$ with the milling time shows predictable changes of the total life at a certain machining moment.

Due to the limited samples of wear data in milling process, the predicted tool life $\bar{t}_j$ per tooth has a fluctuation in a certain degree. The dotted horizontal line in Fig. 9 represents tool average life $\bar{t}$ listed in Table 2. Taking the tool average life $\bar{t}$ into consideration, the parameters (intrinsic amplitude A, the growth frequencies ν_E and ν_L) in Eq. (11) are identified with the experimental data of tool wear. It is observed that the maximum error of predicted tool life after an initial milling period is less than 1–2 min, which means that the tool life can be predicted from tool flank wear per tooth in a short period of initial milling time. For example, a minimum tool life predicted of each tooth is achieved in 5 min after a significant peak or valley in the initial short period (less than 1 min) of first set, as shown in Fig. 9a. The fluctuating of tool life $\bar{t}_j$, obtained from the wear model on each tooth, indicates the instability of the prediction, which is derived from the disequilibrium of the wear rate on each tooth. When the predicted tool life of one tooth is decreasing with the time progression, the wear rate on it is accelerating. Otherwise, the flank wear on that tooth is slowing down. The tool life $\bar{t}$ shows an appropriate prediction which explains the overall machining conditions. In this sense, the tool life can be predicted conveniently and accurately by the generic wear model with adjustable coefficients, and it can be used in real-time machining processes to estimate the tool life expectation efficiently at specific flank wear status.

3.3. The force model comparison and validation

Based on the instantaneous milling force of each flute in Eq. (5), the milling force $F_{\mathbf{M}}(t)$ on a milling cutter, which is obtained from the mechanical force model, is equal to the modulus after summation $\boldsymbol{F}_{\mathbf{M}}(t)$ of the force vector $\boldsymbol{F}_{\mathbf{M}j}(t)$, given as:

$$F_{\mathbf{M}}(t) = |\boldsymbol{F}_{\mathbf{M}}(t)| = \sum_{j=1}^{N_t} \boldsymbol{F}_{\mathbf{M}j}(t) \tag{16}$$

The error δ_F between milling model force $F_{\mathbf{M}}$ in equation (16) and the experimental measurement $F_{\mathbf{O}}$ is given as:

$$\delta_F = (F_O - F_M)/F_O \tag{17}$$

Based on the experimental data of milling force $F_{\mathbf{O}}$, the milling force coefficients $\boldsymbol{K}$ (K_{tc}, K_{rc}, and K_{ac}) in the mechanical model $F_{\mathbf{M}}$ are obtained by a fast calibration algorithm for identification of $\boldsymbol{K}$. The absolute values of $\boldsymbol{K}$ in the t-, r-, and a-axes increase with the milling time [31], as shown in Fig. 10. The Fig. 11 shows that the error δ_F of each milling pass in

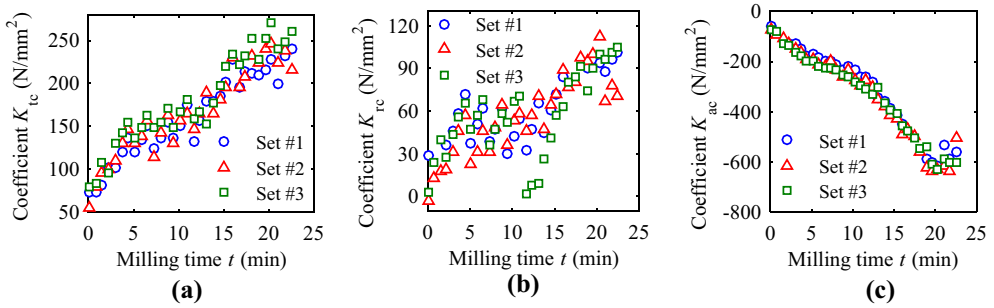

Fig. 10. The milling force coefficients K_{tc}, K_{rc}, and K_{ac} in the mechanical model $F_{\mathbf{M}}$ with experimental data, corresponding to milling time. The coefficients are obtained as in Ref. [31].

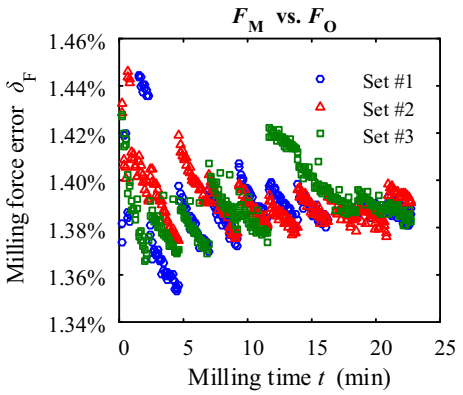

Fig. 11. The error of F_M vs. F_O in the tests. The force F_O is the experimental data, and the force F_M is calculated by Eq. (16).

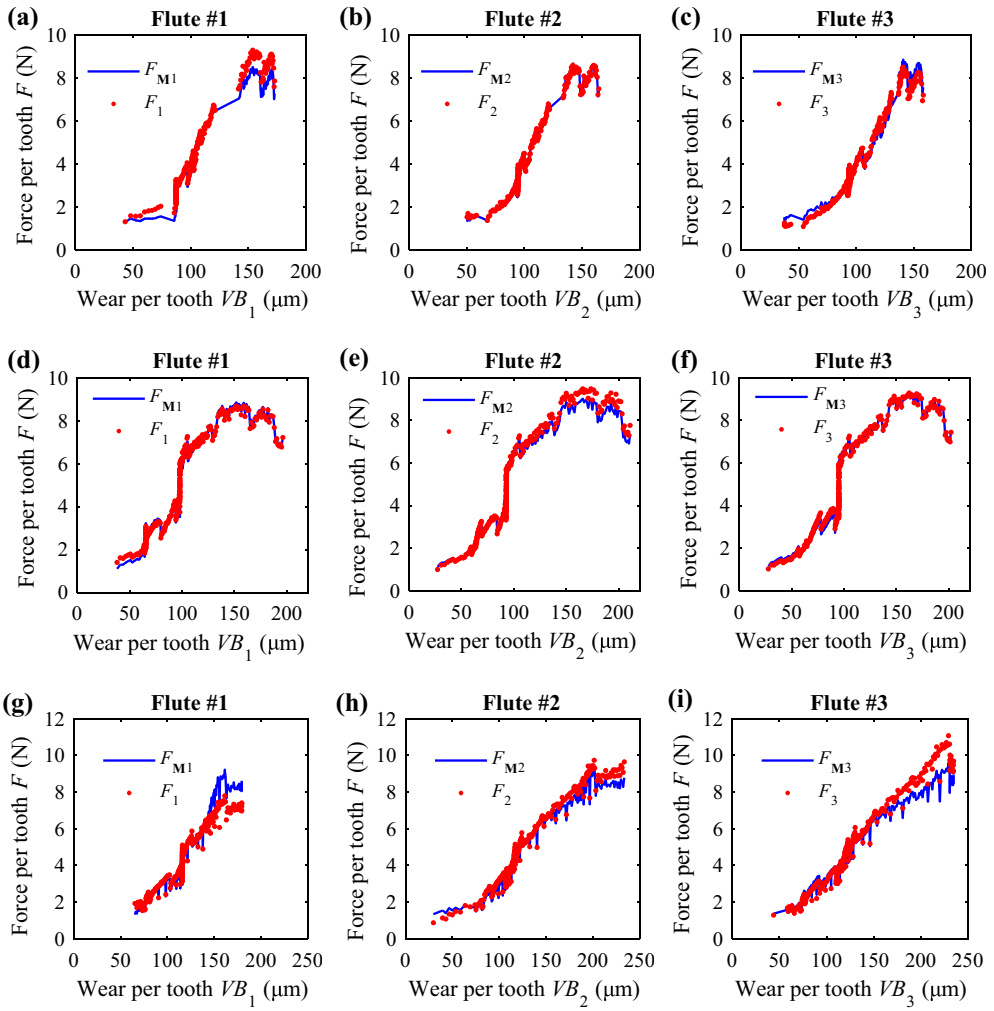

Fig. 12. Milling force F_{Mj} vs. F_j with tool flank wear per tooth in the set (a–c) #1, (d–f) #2 and (g–i) #3 of test 22, obtained from two methods of the mechanical milling force model and the generic tool flank wear model in Eqs. (15a) and (15b) individually.

each set experiment is not more than 1.46%. The trend of the error is interval decreases. The value of the error is lager in the initial milling time than the follow-up time, and there is not obvious fluctuating on the overall values. So it is revealed that the mechanical milling force model is robust over the entire milling time. It is reasonable to compare the two sets of milling force, F_{Mj} and F_j, which are obtained from the mechanical force model and the generic tool flank wear model, respectively.

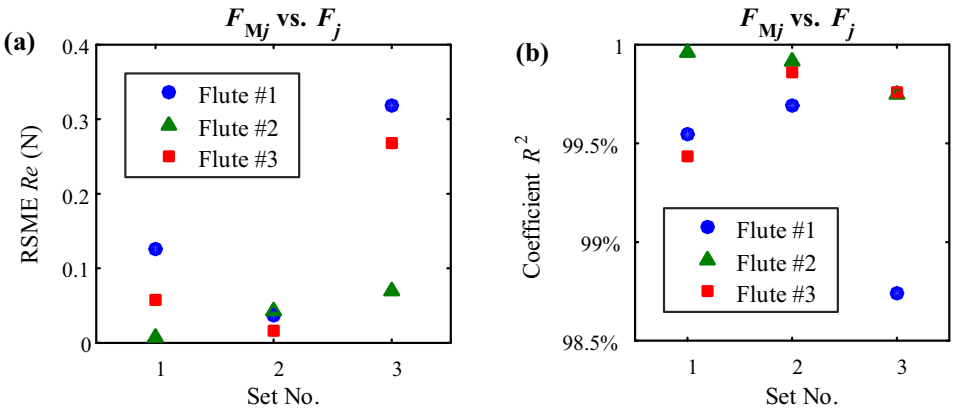

Fig. 13. Statistical results (a) RMSE and (b) coefficient of determination of F_{Mj} vs. F_j in the tests. The forces F_{Mj} and F_j are individually calculated by Eqs. (15a) and (15b).

The milling force $F_{\mathbf{M}j}$ in Eq. (15a) and F_j in Eq. (15b) with the tool flank wear VB_j per tooth of three sets of test 22 are shown in Fig. 12. It can be seen from the results that two sets of curves of $F_{\mathbf{M}j}$ and F_j vs VB_j are very close, and the interference of statistical error points is eliminated commendably by the latter method, as shown in Fig. 12a–c. While tool flank wear VB_j per tooth is lower value in the initial milling time, estimation milling force F_j is not significantly different with each tooth, and F_j increases slowly. With increasing of milling time, F_j increases suddenly when VB_j is between 80 and 120 μm in three sets respectively, which is evident particularly in the second set experiment, as shown in Fig. 12d–f, that is, F_j is increased by more than 5 N. According to VB_j with milling time in Fig. 7, the sudden increase phenomenon of milling force vs VB_j is occurred in the steady state zone (II) wear stage, where tool flank wear is increasing very slowly. After that, the increase rate of milling force vs VB_j is keeping at a higher value stably, and the difference between milling force on each tooth is more obvious causing by constant accumulation of tool run-out. For example, the difference of F_1 with F_2 or F_3 in the third set is more than 5 N in later milling time period, as shown in Fig. 12g–i, which means that the increase rate of milling force in the accelerated wear zone (III) wear stage is similar with VB_j. Accordingly, the flank wear in the first flute is worse than the second and the third ones. It suggests that the status of tool flank wear VB_j per tooth can be reflected by estimation milling force F_j, whose relation can be determined by the force model in Eq. (15a) and the model with wear factor in Eq. (15b).

The root mean square error (RMSE) and coefficient of determination (R^2), between the predicted milling force F_j and the instantaneous milling force $F_{\mathbf{M}j}$ per tooth of each set experiment are shown in Fig. 13. The RMSEs in all sets are not more than 0.35 N, which is far less than milling force per tooth over milling time, as shown in Fig. 12. It can be seen that there is little difference of RMSE on each flute in each set experiment. The coefficients R^2, which is the square of the correlation coefficient (R) used to measure the agreement between two methods, are more than 98.5% in all sets as shown in Fig. 13b. It indicates that the generic wear prediction model with adjustable coefficients has rationality and accuracy on prediction of milling force per tooth.

The results indicate that the milling force per tooth can be effectively estimated according to tool flank wear per tooth. The tool flank wear model with adjustable coefficients can not only simplify wear analysis, but also is a method to distribute instantaneous milling force on each tooth, considering with the factor λ_j. The parameters in the wear model, i.e., the identified intrinsic amplitude A and the growth frequencies v_E and v_L, can be adapted to various machining conditions by adjusting the corresponding numerical relations with experimental data. So the wear model can be generalized and applicable to varied milling conditions.

4. Conclusions

A generic explicit model with adjustable coefficients has been developed for tool flank wear in high speed ball-nose end milling. It is based on the nature of the first and second order differentiation properties of tool flank wear curve, and the logarithmic and cubic polynomials are applied to model the earlier and later zones of wear curves. It has been shown that the coefficient of determination of the generic wear model is no less than 95% against the experimental data. At the same time, with inclusion of wear factor, the milling force per tooth has been modeled and validated according to the instantaneous force model, with fitting error less than 1.46% with the experimental data. The results have shown that the tool average life can be monitored and predicted online with high accuracy by considering tool wear status in this study. Due to the adjustability of the model coefficients, this approach could be conveniently generalized and applicable to varied milling conditions.

Acknowledgements

This project is supported by the CAS100 Talents Program, the Chinese Academy of Sciences (CAS), and the National Natural Science Foundation of China (Grant No. 51475443).

Appendix A. The derivation of Eq. (8)

The exact integrated results of the wear function in Eq. (7) is:

$$w(t) = \int [a_1/(t+b_1) + c_1]dt + \iint (a_2 t + b_2)\mathrm{d}t_2 = [a_1 \ln(t+b_1) + c_1 t + D_1] + \left(\frac{a_2 t^3}{6} + \frac{b_2 t^2}{2} + D_2 t + D_3\right)$$
$$= a_1 \ln\left(\frac{1}{b_1}t + 1\right) + \frac{a_2}{6}t^3 + \frac{b_2}{2}t^2 + (c_1 + D_2)t + D_1 + D_3 + a_1 \ln b_1 \quad \text{(a)}$$

where D_1, D_2, and D_3 are integral constants. In the ideal theoretical tool wear model, the fresh tool is not worn. So there is a boundary condition:

$$w(0) = 0 \quad \text{(b)}$$

With the equations (a) and (b), the constants are given as:

$$D_1 + D_3 = -a_1 \ln b_1 \quad \text{(c)}$$

Hence, the wear function is equal to:

$$w(t) = a_1 \ln\left(\frac{1}{b_1}t + 1\right) + \frac{a_2}{6}t^3 + \frac{b_2}{2}t^2 + (c_1 + D_2)t \quad \text{(d)}$$

According to the characteristics of two preference transition wear functions w_E and w_L we given, which describe the initial and significant wear stages successively. The effect of the adhesive wear and three-body abrasive wear in the initial wear stage is tiny (virtually invisible) [25]. Hence, the supplementary boundary condition is given as:

$$w_L''(0) = 0 \quad \text{(e)}$$

With the equations (a), (d), and (e), the wear function is derived as:

$$w(t) = a_1 \ln\left(\frac{1}{b_1}t + 1\right) + \frac{a_2}{6}t^3 + (c_1 + D_2)t \quad \text{(f)}$$

Simplifying the equation (f) and removing low order variables t, which have less effect than two-higher order variable t^3 on the tool wear in the significant wear stage, the tool wear model is simplified as:

$$w(t) = a_1 \ln\left(\frac{1}{b_1}t + 1\right) + \frac{a_2}{6}t^3 \quad \text{(g)}$$

Substituting the parameters in the Eq. (g):

$$A = a_1; \quad B = \frac{1}{b_1}; \quad C = \frac{a_2}{6} \quad \text{(h)}$$

With the Eqs. (g) and (h), the tool wear model is rewritten as:

$$w(t) = A \ln(Bt + 1) + Ct^3 \quad \text{(i)}$$

which is the Eq. (8) in the Section 2.3.

References

[1] G. Totis, G. Wirtz, M. Sortino, D. Veselovac, E. Kuljanic, F. Klocke, Development of a dynamometer for measuring individual cutting edge forces in face milling, Mech. Syst. Signal Process. 24 (6) (2010) 1844–1857.
[2] Wit Grzesik, Advanced Machining Processes of Metallic Materials, second ed., Elsevier, 2017.
[3] D. Zhu, X. Zhang, H. Ding, Tool wear characteristics in machining of nickel-based superalloys, Int. J. Mach. Tool. Manuf. 64 (1) (2013) 60–77.
[4] X. Cui, J. Zhao, Y. Dong, The effects of cutting parameters on tool life and wear mechanisms of CBN tool in high-speed face milling of hardened steel, Int. J. Adv. Manuf. Technol. 66 (5) (2013) 955–964.
[5] C.Y. Wang, Y.X. Xie, Z. Qin, H.S. Lin, Y.H. Yuan, Q.M. Wang, Wear and breakage of TiAlN- and TiSiN-coated carbide tools during high-speed milling of hardened steel, Wear 336–337 (8) (2015) 29–42.
[6] A. Sharman, R.C. Dewes, D.K. Aspinwall, Tool life when high speed ball nose end milling Inconel 718, J. Mater. Process. Technol. 118 (1–3) (2001) 29–35.
[7] R. Teti, K. Jemielniak, G. O'Donnell, D. Dornfeld, Advanced monitoring of machining operations, CIRP Ann. Manuf. Technol. 59 (2) (2010) 717–739.
[8] J.A. Duro, J.A. Padget, C.R. Bowen, H.A. Kim, A. Nassehi, Multi-sensor data fusion framework for CNC machining monitoring, Mech. Syst. Signal Process. 66–67 (1) (2016) 505–520.
[9] D.A. Tobon-Mejia, K. Medjaher, N. Zerhouni, CNC machine tool's wear diagnostic and prognostic by using dynamic Bayesian networks, Mech. Syst. Signal Process. 28 (4) (2012) 167–182.

[10] R. Hood, C.M. Johnson, S.L. Soo, D.K. Aspinwall, C. Sage, High-speed ball nose end milling of burn-resistant titanium BuRTi alloy, Int. J. Comput. Integr. Manuf. 27 (2) (2014) 139–147.
[11] I. Lee, V. Bajpai, S. Moon, J. Byun, Y. Lee, H.W. Park, Tool life improvement in cryogenic cooled milling of the preheated Ti-6Al-4V, Int. J. Adv. Manuf. Technol. 79 (1) (2015) 665–673.
[12] M.J. Bermingham, W.M. Sim, D. Kent, S. Gardiner, M.S. Dargusch, Tool life and wear mechanisms in laser assisted milling Ti-6Al-4V, Wear 322–323 (2) (2015) 151–163.
[13] M.A. Rodrigues, A. Hassui, R.H.L.D. Silva, D. Loureiro, Tool life and wear mechanisms during Alloy 625 face milling, Int. J. Adv. Manuf. Technol. 85 (5) (2016) 1–10.
[14] R. Yan, R.X. Gao, Approximate Entropy as a diagnostic tool for machine health monitoring, Mech. Syst. Signal Process. 21 (2) (2007) 824–839.
[15] M. Nouri, B.K. Fussell, B.L. Ziniti, E. Linder, Real-time tool wear monitoring in milling using a cutting condition independent method, Int. J. Mach. Tool Manuf. 89 (2) (2015) 1–13.
[16] M. Lamraoui, M. Thomas, M.E. Badaoui, Cyclostationarity approach for monitoring chatter and tool wear in high speed milling, Mech. Syst. Signal Process. 44 (1–2) (2014) 177–198.
[17] W. Wang, Y.S. Wong, G.S. Hong, Flank wear measurement by successive image analysis, Comput. Ind. 56 (8–9) (2005) 816–830.
[18] C. Drouillet, J. Karandikar, C. Nath, A.C. Journeaux, M.E. Mansori, T. Kurfess, Tool life predictions in milling using spindle power with the neural network technique, J. Manuf. Process. 22 (2016) 161–168.
[19] N. Ghosh, Y.B. Ravi, A. Patra, S. Mukhopadhyay, S. Paul, A.R. Mohanty, Estimation of tool wear during CNC milling using neural network-based sensor fusion, Mech. Syst. Signal Process. 21 (1) (2007) 466–479.
[20] K. Zhu, Y.S. Wong, G.S. Hong, Multi-category micro-milling tool wear monitoring with continuous hidden markov models, Mech. Syst. Signal Process. 23 (2) (2009) 547–560.
[21] F.A. Niaki, M. Michel, L. Mears, State of health monitoring in machining: Extended Kalman filter for tool wear assessment in turning of IN718 hard-to-machine alloy, J. Manuf. Process. 24 (2) (2016) 361–369.
[22] K. Orra, S.K. Choudhury, Development of flank wear model of cutting tool by using adaptive feedback linear control system on machining AISI D2 steel and AISI 4340 steel, Mech. Syst. Signal Process. 81 (12) (2016) 475–492.
[23] E. Usui, T. Shirakashi, T. Kitagawa, Analytical prediction of cutting tool wear, Wear 100 (1–3) (1984) 129–151.
[24] X. Yang, C.R. Liu, A new stress-based model of friction behavior in machining and its significant impact on residual stresses computed by finite element method, Int. J. Mech. Sci. 44 (4) (2002) 703–723.
[25] M.C. Shaw, Metal Cutting Principles, second ed., Oxford University Press, Oxford, 2005, pp. 178–181.
[26] F.W. Taylor, On the art of cutting metals, Trans. ASME 28 (1907) 31–350.
[27] M.S. Kasim, C.H.C. Haron, J.A. Ghani, M.A. Sulaiman, M.Z.A. Yazid, Wear mechanism and notch wear location prediction model in ball nose end milling of Inconel 718, Wear 302 (1–2) (2013) 1171–1179.
[28] G. Zhang, S. To, G. Xiao, Novel tool wear monitoring method in ultra-precision raster milling using cutting chips, Precis Eng. 38 (3) (2014) 555–560.
[29] H. Li, G. He, X. Qin, G. Wang, C. Lu, L. Gui, Tool wear and hole quality investigation in dry helical milling of Ti-6Al-4V alloy, Int. J. Adv. Manuf. Technol. 71 (5) (2014) 1511–1523.
[30] Z. Zhu, R. Yan, F. Peng, X. Duan, L. Zhou, K. Song, C. Guo, Parametric chip thickness model based cutting forces estimation considering cutter runout of five-axis general end milling, Int. J. Mach. Tool Manuf. 101 (2) (2016) 35–51.
[31] K. Zhu, Y. Zhang, Modeling of the instantaneous milling force per tooth with tool run-out effect in high speed ball-end milling, Int. J. Mach. Tool Manuf. 118–119 (1) (2017) 37–48.